POLITECNICO
MILANO 1863

SCUOLA DI INGEGNERIA INDUSTRIALE
E DELL'INFORMAZIONE

Executive Summary of the Thesis

Generation and Clustering of Weak Stability Boundaries for Cislunar Escapes

Laurea Magistrale in Space Engineering - Ingegneria Spaziale

Author: Enrico Bassissi

Advisor: Prof. Michèle Lavagna

Co-advisor: Andrea Pasquale

Academic year: 2021-2022

1. Introduction

The scientific and commercial exploitation of the cislunar environment for both manned and unmanned missions will increase in the next few decades, opening the frontier of space for increasingly daring and challenging explorations. Those ambitious missions face complex dynamics that cannot be adequately addressed with classical trajectory design techniques. New methodologies for trajectory design in multi-body environment have to be leveraged, pushing the boundaries toward new techniques. For example, the low-energy trajectory design represents one of the promising directions of future developments. Weak Stability Boundaries (WSB) theory [1] takes full advantage of the dynamic effects of two or more gravitating bodies, and it has been already employed in some missions during the last few decades, such as HITEN, SMART-1, ARTEMIS, GRAIL, and others.

1.1. Objective

The thesis will focus on escape trajectories from the cislunar space [2], characterising their dynamical behaviour in the four-body problem (BCR4BP) framework. It will address the problem to design a transfer from the Earth-Moon Libration Points L_2 to a destination object outside the cislunar environment, generating initial guess solutions that leverage and exploit weak stability boundaries in a reversed approach.
Techniques from unsupervised machine learning may aid in summarising and understanding the solution space inferring undetected patterns [4] with the specific application of identifying a set of motion primitives that represents a family of orbits. In particular, it will expand the knowledge about unsupervised clustering of open (escape) trajectories by exploiting geometrical and parametric features, in a complex and sensitive environment such as BCR4BP, applying the weak stability boundaries theory to a case study scenario related to escape the cislunar environment to reach Near Earth Asteroid.

1.2. Dynamical Model - BCR4BP

In this thesis, the design of trajectories in the cislunar space is performed leveraging the BCR4BP framework. This model assumes that the two primaries P_1 and P_2 revolve in circular orbits about their barycentre (B_1) and B_1 moves in circular orbits around the centre of mass of the whole system, B_0.
The BCR4BP can be seen from two different but identical frame: one taking as reference the Sun-Earth system and the other synodic with Earth-Moon system. Consequently, the equations of motion can be written in the Sun-Earth synodic frame or in the Earth-Moon one [3].

The first case will be the one described here since it's the most represented in this thesis. The equations of motion considers the the Moon as a perturbation of the Sun-Earth CR3BP and can be derived from a pseudo-potential function ($\underline{\Upsilon}$), reported in eq. (1) and continuing in eq. (2). Here, $(\dot{\cdot})$ and $(\ddot{\cdot})$ denotes the first and the second derivatives with respect to the non-dimensional time and $\partial(\times)/\partial(\cdot)$ indicates the partial derivative of a function $(\times)$ with respect to a variable $(\cdot)$. The terms in the equations are: θ_{EM} is the Moon angular position which respect to the Sun-B_1 $\underline{x}$ synodic axis; $\underline{\mu}$ denotes the mass ratio of the Sun-(Earth+Moon) CR3BP and with $\tilde{\mu}$ the one of the Earth-Moon CR3BP; and r_{43}, r_{13}, and r_{23} represents this time respectively the distance of the particle from the Sun, the Earth and the Moon.

$$\underline{\Upsilon} = \frac{1}{2}(\underline{x}^2 + \underline{y}^2) + \frac{1-\underline{\mu}}{r_{43}} + \frac{\underline{\mu}(1-\tilde{\mu})}{r_{13}} + \frac{\underline{\mu}\tilde{\mu}}{r_{23}} \quad (1)$$

$$\begin{cases} \ddot{\underline{x}} = 2\dot{\underline{y}} + \dfrac{\partial \underline{\Upsilon}}{\partial \underline{x}} \\ \ddot{\underline{y}} = -2\dot{\underline{x}} + \dfrac{\partial \underline{\Upsilon}}{\partial \underline{y}} \\ \ddot{\underline{z}} = \dfrac{\partial \underline{\Upsilon}}{\partial \underline{z}} \end{cases} \quad (2)$$

2. Initial Conditions Generator

2.1. Control Surface

To design the trajectories under discussion, the problem has been splitted into two separated regions, decoupling the design between the Earth-Moon region up to a given Control Surface radius, i.e. the *Inner Problem*, and the heliocentric trajectory leg, from the selected Control Surface radius up to the target interception, i.e. the *Outer Problem*.
This idea is built upon the similar concept developed in literature of the Sphere of Equivalence (SOE). However, the switching surface exploited in this work is an abstract concept, a spherical interface surface, not a physical one. Introducing this simplification enable the possibility to generate Outer Problem and Inner Problem arcs independently. A switching surface, centred in the Earth-Moon Barycenter B_1 with radius approximately $2 \cdot SOI_{Earth-Moon} =\cong 2 \cdot 10^6$ km is then considered.
On the switching surface, vector quantities that has to be matched can be generally denoted with q^+ if belonging to the Outer Problem, and q^- if associated to the Inner Problem.
From this, the vectorial difference between the Inner and the Outer Problem general vectors can be defined as $\Delta\underline{q} = \underline{q}^+ - \underline{q}^-$ and their angular difference angle through the cosine law.

2.2. Starting Point and Free Variables

In the BCR4BP SB_1 framework, L_2 is derived from the rotation of the state generated in CR3BP. In this way, L_2 moves rigidly with the Earth-Moon conjunction axis, on the other side of the Moon, so that it can be identified uniquely through the same DOF of the Earth and Moon themselves, the Moon angle θ_{EM}.
Analysis performed through the use of the dynamical substitute of L_2 in BCR4BP instead of the CR3BP derived L_2 led to similar results as the one presented here. Therefore the decision to simplify the work and alleviate one DOF more at the beginning of the dynamical exploration.
The other DOFs acting on the system are the impulse ΔV applied at L_2 to exit from its "equilibrium" position and α the angle at which this perturbation is applied with respect to the radial direction θ_{EM}.
The free variables are depicted in fig. 1

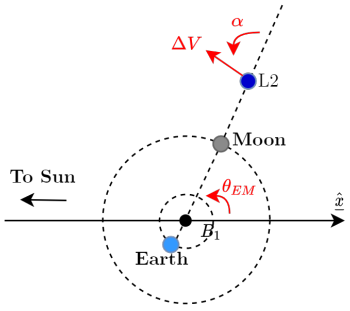

Figure 1: Starting Point and Free Variables, the DOFs of the problem θ_{EM}, ΔV, α are shown in red.

The ranges of evaluation in this step of the analysis are reported in table 1:

Table 1: Initial DOFs Ranges of Evaluation

θ_{EM} [rad]	ΔV [m/s]	α [rad]
$[0, 2\pi)$	$[1, 200]$	$[0, \pi/2]$

2.3. Inner Condition Set and Considerations

These free variables permutations applied to the system, have been propagated for a time span of 1 year. Many aspects have been tracked in order to proceed with a post-processing step later and prune the large amount of data to make the following phases more efficient, mainly: **Escapes** from the cislunar space, crossing the Control Sphere distance R_c without returning in the considered time; **EMB Apoapsis**, if the trajectory has an apoapsis in the SB_1 frame with respect to B_1 in the region near the Control Sphere at 1.5/2 million km, then it's considered a valid WSB.

The main objectives of this phase were to focus on trajectories that are already known to satisfy the constraints of the analysis to be done, to gain insights from the dynamical behaviour of the environment and understand which parameters had more or less effect on the overall analysis to focus the effort on the more relevant ones.

From initial results was clear that the WSB Escape trajectories were mainly reliant on θ_{EM} and ΔV DOFs and α was less effective, especially at low $\Delta V < 50$ m/s, as it's possible to see in fig. 2. The meaning of this behaviour has been addressed to the fact that for lower ΔV, the impulse was mainly dedicated to getting out of the nominal L_2 trajectory in an almost natural evolution, following approximately the associated unstable invariant manifolds direction.

Another result on the free variables analysis is that the valid WSB Escape trajectory generates only with θ_{EM} in the II and IV quadrants of the xy plane with B_1 as origin. This effect was correlated to the fact that trajectories starting in other quadrants were rapidly evolving toward direct escape and not through a WSB. This effect was also more defined for the low ΔV ranges selected.

The final set of free variables is given in table 2.

Table 2: DOFs Ranges of Evaluation After First Post-Processing

θ_{EM} [Quadr.]	ΔV [m/s]	α [-]
II-IV	[1, 50]	Removed

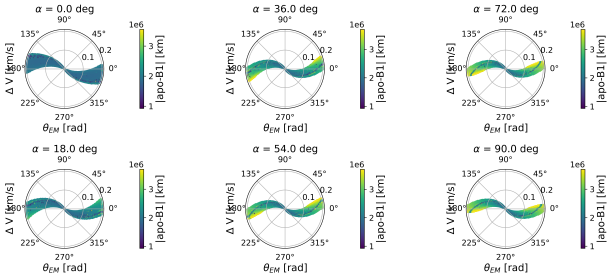

Figure 2: WSB Escape Trajectory Existence at Varying α, Polar Plot

3. Machine Learning Clustering

Processing all the trajectories together can be chaotic, leading to inconclusive and unrepeatable results. The trajectories are too many to be processed as unique bunch or to be separated by hands from a researcher, also in perspective of increasing number of propagations through the use of GPGPU programming. The best tool to approach this sort of problems is indeed Machine Learning.

3.1. Algorithm and Setup

In particular, in this case study Machine Learning is used to perform the automatic clustering of the trajectories, using the algorithm *DBSCAN* (Density-Based Spatial Clustering of Applications with Noise). *DBSCAN* views clusters as dense area of the vector space separated by areas of low density. There are two parameters to the algorithm, *min_samples* and *eps*, controlling respectively the local neighbourhood of the points and how tolerant the algorithm is towards noise.

For what concerns this orbits clustering, following [4], the selected features space is a geometric realisation of the trajectory, directly through the states in cartesian coordinates, positions with respect to B_1 and velocities, equally spaced in time along the trajectory and can be defined as in eq. (3).

$$\underline{f} = \left[\frac{(x_m - x_{B1}) - x_{min}}{x_{max} - x_{min}}, \frac{y_m - y_{min}}{y_{max} - y_{min}}, \frac{v_{x,m} - v_{x,min}}{v_{x,max} - v_{x,min}}, \frac{v_{y,m} - v_{y,min}}{v_{y,max} - v_{y,min}} \right] \quad (3)$$

where m goes from 0 to the number of discrete positions sampled along the trajectory. All the components have been normalised between the maximum and the minimum value to be in the range [0, 1].

DBSCAN is very sensitive to the values of *eps* and *min_ samples*. For this reason, an optimisation process has been devised in order to avoid the difficult and repetitive manual tuning of the parameters. *PSO* (Particle Sworm Optimization) algorithm was used.
To evaluate the quality of clustering solutions it was used an internal validity criteria, having only the information intrinsic to the data. The density-based clustering validation (DBCV) index was applied: it's governed by the maximum internal sparseness of each cluster and the highest density regions between pairs of clusters. From this, the validity index can be computed and its value varies in ranges [-1, 1], with -1 being completely not valid and 1 cluster that is coherent within itself and with the other clusters. This was then selected as the performance metric to use in the optimisation process.

3.2. Clustering Results

The families are presented here below, divided by the quadrant of starting θ_{EM} (II or IV) to ease the readability of the results, the comprehension of the phenomena under study and to follow the natural subdivision obtained in section 2.3. The final trajectories plot in *xy* plane are here shown in fig. 3 and fig. 4, as detected by the *DBSCAN* optimised algorithm, respectively for θ_{EM} in the II or in the IV Quadrant. For each cluster, some random trajectories taken as representatives are plotted to show the general behaviour and evolution within the family.

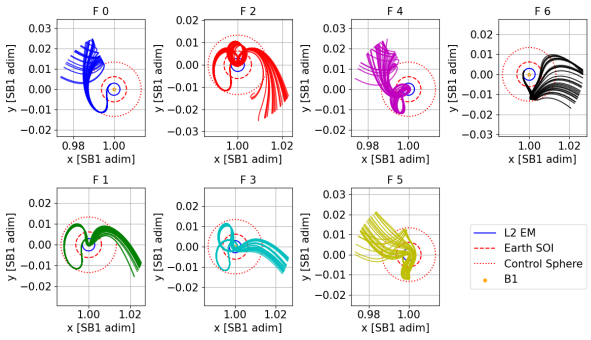

Figure 3: *xy* plot of Families Trajectories Detected through Clustering for F II Q

As can be seen from the plots, the variety of trajectories is high, with different geometrical and dynamical behaviours, manifestation of the complex and sensitive environment under study. It's interesting to notice that even considering only the families of the II Quadrant it's possible to reach targets of the inner and outer heliocentric space. The same geometrical and dynamical considerations can be done for both the groups, noticing that the trajectories reflect the quasi-symmetric behaviour of the BCR4BP framework. Among the dynamical characteristics of the trajectories, an important aspect is that the trajectories reach on average a $V_\infty \sim 1$ km/s order of magnitude by only applying a small impulse perturbation at departure of the order of tens of m/s.

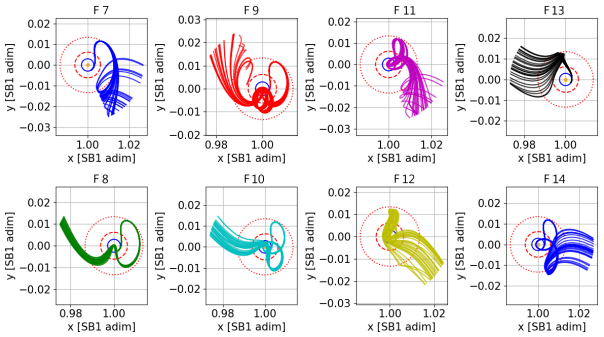

Figure 4: *xy* plot of Families Trajectories Detected through Clustering for F IV Q

The best hyper-parameters and average performance factors have been reported in table 3: *eps*, *min_ samples*, the average Validity Index, scoring positively and toward 1 for all the clusters, and the percentage of coverage of the datapoint clustered, successfully kept above the 80% threshold considered a balanced optimisation.

Table 3: DBSCAN Hyper-parameters for Families in II and IV Quadrant

	eps	***min sample***	**avg VI [-]**	**Coverage [%]**
IIQ	0.0574	106	0.779	81.24
IVQ	0.0437	118	0.850	80.08

4. Initial Guess Generator

The final objective of this analysis is to produce an end-to-end technique to generate initial guesses for escape trajectories from cislunar environment, with embedded weak stability boundaries features, matching an external requested condition towards NEA objects.

4.1. Targets and Case Study

To start, the NEAs characteristic orbital parameters have been analysed through the NASA's

Small Body DataBase. Since the possible targets are many and a specific asteroid is not the main objective of this thesis work, the decision made was to not choose one specific target but one average representative of each group, considering the average orbital elements in a, e, i, M. With these results, a database of Outer Problem targets was generated, upon which the transfer trajectories were designed. All the targets have been evaluated and the pipeline was robust enough to find solutions for every case reported. To ease the explanation and the description of the method, one relevant case study is extracted selecting one NEA case, a member of the *Amor* group, whose parameters are in table 4, assuming the reference Epoch ET_0 as 2024-01-01 00:00:00.

Table 4: *Amors* Target Parameters

a [AU]	e [-]	i, Ω, ω [deg]	M [deg]
1.3645	0	0	196.2

The set of transfers is generated assuming Two-Body motion of the Earth and the target body around the Sun, exploiting Lambert's arc method and the Porkchop Plot analysis, representing the ΔV cost of that manoeuvre for a rendezvous mission.
Thus far the problem is still under the 2BP framework, but the Inner Problem trajectories are provided in BCR4BP. For this reason, the transfers identified in the previous step need to be back-propagated in BCR4BP, starting from the fixed arrival position to the target, back in time to the Earth departure. At this point there will be some inconsistencies with the match given by the 2BP analysis, moving the departure point away from the Earth. For this reason, a small step of Differential Correction was used, to bring back the starting point at the Control Sphere. From this results, the newly corrected Outer Problem trajectories form the proper database related to the Outer conditions to be matched by the Inner Problem WSB families trajectories.

4.2. Patching Procedure

Among the possible solutions is then selected the one that minimise the sum of the Lambert 2BP and the BCR4BP trajectory differential correction, in order to get the true minimum among them. For each family of the Inner Problem, a patching algorithm has been developed in order to find the best trajectory and the best one-impulse control to give at a specified point to reach the wanted Outer Problem parameters, and it will be described here following.
1. One trajectory representative of the family is selected, privileging the ones with a pericentre.
2. A spectrum of manoeuvres is applied to that trajectory at its B_1 pericentre, in a variety of impulse magnitudes 0.5 and 2 km/s and in a variety of directions, radial, tangential and anti-radial (90°, 0°, -90°), as shown in fig. 5. A matrix of possible controlled trajectory is constructed and the closest to the possible match is chosen.

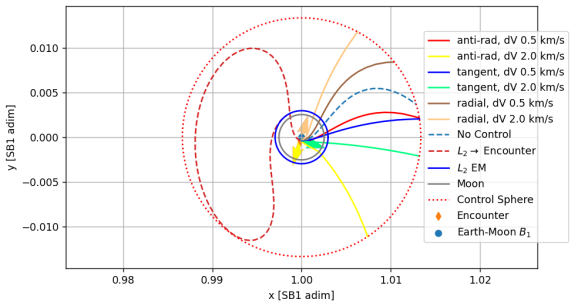

Figure 5: Control Spectrum Example and Reachable Span of Solutions

3. If the family has a geometrical behaviour that brings all its trajectories toward a region of space not suited for that particular matching ($\Delta\theta_{R_c}^{IP-OP} > \pi/4$), the family is discarded a priori from the analysis.
4. This spectrum control solution selected is then fed to another DC step, to actually meet the condition requested at the Control Sphere and produce a valid continuous path. This optimisation proceeds minimising the residue related to the elements described in fig. 6. These final solutions are saved in a database in order to be then post-processed during the final selection.
5. Among all the families solutions, the one that has less final sum residue of the final DC step, is selected as best of all to patch the Outer Problem.

4.3. Patching Results

For each case there are more than one solutions. For the *Amor* NEA selected as case study, only one reference good example is reported here to show the outcome of the pipeline.
The conditions deriving from the Outer Problem request at R_c are reported: $V_\infty = 2.479$ km/s,

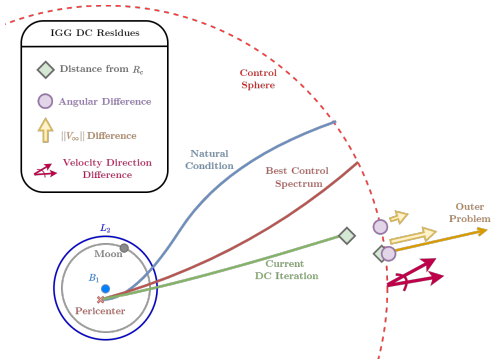

Figure 6: Depiction of the Initial Guess Generation Differential Correction Procedure

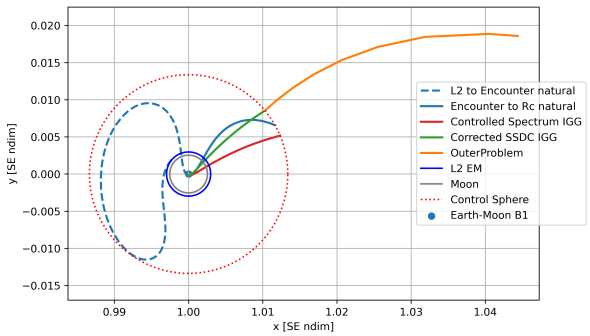

Figure 7: Best Solution Patching NEA Amor Selected - Family **F1**

$\theta_{pos} = 39.71°$ and the angle of the velocity vector is $\hat{\theta}_{vel} = 47.20°$.
Per each family, from the control spectrum propagation, the algorithm evaluates the selection metrics of the DC step. Not all the families made it through this filtering, due to the geometrical filtering. After this passage, only 9 out of the total 14 families survived and have to be evaluated and corrected in order to yield a truly comparable result.
Following the procedure, the optimisation can take place, and the parameters are reported in table 5: the control spectrum entry guesses and the optimised values for the α, ΔV and TOF.

Table 5: Procedure Parameters for Family **F1** Results

	α [deg]	**ΔV** [km/s]	**TOF** [d]
Control Spectrum	0.0	0.5	9.39
Optimal Data	65.21	1.221	8.50

In fig. 7 the best condition of patching is shown in a cartesian xy projection. The difference in direction of the velocity is only 10.65°; the control applied is well below the limit set and the lowest among the solutions; the V_∞ is completely matched and also the position on the Control Sphere; the TOF has been reduced since the dynamic is faster.

5. Conclusions

To conclude, in this thesis a new methodology for the generation and clustering of weak-stability boundaries escape trajectories have been presented, along with the application for a relevant NEA case.
The method appears to be flexible and efficient, since the escape conditions can be built once and then used for different mission scenarios. Moreover, the clustering into families gives the possibility to filter the database upon certain characteristics a priori of the optimisation, ultimately leading to a smaller subset of valid and cost-effective initial guesses to be processed. The application of the patching conditions, passed through the control spectrum step, guarantees a fast convergence of the differential correction procedure, allowing for a fast identification of suitable escape trajectories from the cislunar space.

References

[1] E. Belbruno and J. Miller. A ballistic lunar capture trajectory for the japanese spacecraft hiten. *Jet Propulsion Laboratory*, 1990.

[2] Andrea Pasquale, Michèle Lavagna, and Florian Renk. Cislunar escape trajectories through patched sun-earth/earth-moon three-body problem. 10 2021.

[3] Stephen T. Scheuerle. Construction of ballistic lunar transfer in the earth-moon-sun system. Master's thesis, Purdue University, West Lafayette, Indiana, USA, May 2021.

[4] Thomas Smith and Natasha Bosanac. Constructing motion primitive sets to summarize periodic orbit families and hyperbolic invariant manifolds in a multi-body system. *Celestial Mechanics and Dynamical Astronomy*, 134, 02 2022.